Appl. Phys. B (2015) 118:511–516
DOI 10.1007/s00340-015-6047-7

Applied Physics B
Lasers and Optics

RAPID COMMUNICATION

Coherent combining of relativistic-intensity femtosecond laser pulses

V. E. Leshchenko · V. A. Vasiliev · N. L. Kvashnin · E. V. Pestryakov

Received: 10 November 2014 / Accepted: 5 February 2015 / Published online: 15 February 2015

Abstract We report on the experimental realization of the peak intensity scaling technique. Coherent combining of relativistic-intensity femtosecond laser pulses is demonstrated for the first time. The original stabilization setup developed by us provides 100 Hz stabilization bandwidth and a 85 mrad root mean square relative phase instability of amplified pulses which enables as high as 93 % efficiency of coherent beam combining under tight focusing. The peak intensity scaling from 3×10^{19} W/cm^2 for the two individual beams to 1.15×10^{20} W/cm^2 for the combined beam is achieved using a *f*/1.2 parabolic mirror. A Strehl ratio of about 0.5 is experimentally obtained without any wavefront correction setup. Currently, it is this work that demonstrates coherent combining of femtosecond pulses with the record pulse parameters, namely with simultaneously the highest peak intensity, highest peak power, highest energy, and shortest duration.

The development of fundamental high-field physics requires the production of a focused intensity above 10^{23} W/cm^2. This intensity is called ultra-relativistic because it can accelerate not only electrons but also ions to the speed of light. A facility delivering such intensity can be used to advance attosecond science, high-energy particle acceleration, secondary radiation generation, and laser-based nuclear physics [1]. There are a number of projects handling the problem, such as ELI (Extreme Light Infrastructure) in Europe [2], XCELS (Exawatt Center for Extreme Light Studies) in Russia [3], and the ultra-high-intensity laser in the Laboratory for Laser Energetics in Rochester, USA [4]. And the coherent beam combining of high-intensity tightly focused femtosecond pulses is a key technique [2–4]. However, thus far, coherent combining of femtosecond pulses has only been demonstrated under focusing by a low-numerical aperture spherical mirror [5, 6]. Therefore, the implementation of the coherent combining of high-intensity laser pulses under tight focusing is of considerable importance and is the subject of this study.

The dual-channel experimental setup is shown in Fig. 1. Seed pulses generated by Ti:Sa laser (Fusion Pro 400, FemtoLasers) are stretched to about 40 ps by an Öffner-stretcher. Details of the stretcher design can be found elsewhere [7]. A three-stage parametric amplification in BBO (first stages and the second stage in the second channel) and LBO (third stages and the second stage in the first channel) crystals is implemented in each channel. The optical parametric amplifiers are pumped by 90 ps pulses at 532 nm wavelength, 10 Hz repetition rate generated by a four-channel Ekspla APL 2106 laser system delivering about 500 mJ in each channel. To pump the first stages nearly 5 % of a pump beam is double split. After amplification, pulses are compressed with Treacy grating compressors based on two gold-coated 1200 l/mm reflective holographic gratings in a two pass configuration. Energies of 75 and 110 mJ are achieved in the first and the second channels, respectively. The tight focusing scheme is shown schematically in Fig. 1a. Two 38-mm beams are focused by a gold-coated off-axis parabolic mirror (Edmund Optics, diameter $D = 76.2$ mm, effective focal length $F = 89.3$ mm, 45°, $F/D = 1.17$ and numerical aperture NA = 0.21). The

V. E. Leshchenko (✉) · V. A. Vasiliev · N. L. Kvashnin · E. V. Pestryakov
Institute of Laser Physics SB RAS, Ac. Lavrentyev's prosp. 13/3, 630090 Novosibirsk, Russia
e-mail: leschenkoslava@gmail.com

V. E. Leshchenko · E. V. Pestryakov
Novosibirsk State University, Pirogova str. 2, 630090 Novosibirsk, Russia

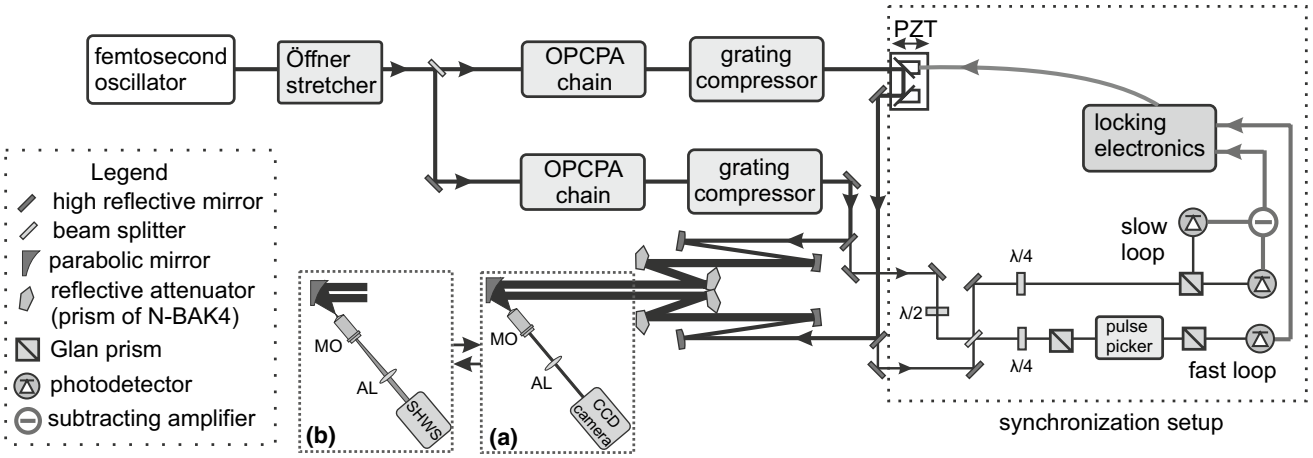

Fig. 1 Experimental setup for the measurement of focal spots (**a**) and wavefronts (**b**): *MO* microscope objective, *AL* achromatic infinity-corrected tube lens, *SHWS* Shack–Hartmann wavefront sensor, *OPCPA* optical parametric chirped pulse amplification, *PZT* piezoelectric transducer, λ/2 and λ/4 wave plates

focal spots are registered by a 12-bit CCD camera (Ophir Optronics Solutions Ltd) through an imaging system consisting of a microscope objective and an achromatic infinity-corrected tube lens with a 20-cm focal length. A field curvature-corrected, apochromatic infinity-corrected microscope objective with a 40 × magnification and a 0.75 numerical aperture is used. Beam attenuation lines are used to prevent air breakdown and optical damage of the objective and the CCD camera by the high-intensity focused beam (Fig. 1). The attenuation of the laser pulses after the amplifier stages and the compressors under full power operation maintains the beam qualities, i.e., the beam profile, the wavefront distortion and the pulse duration. Wavefront aberrations are measured using the same imaging system (Fig. 1b). However, instead of relaying an image from the focus of the parabolic mirror to measure the focal spots, the configuration is adjusted to relay the image of the beam before the parabolic mirror onto a wavefront sensor. The Shack–Hartmann wavefront sensor consists of a 20 × 20 microlenslet array that is coupled to a CCD camera with a 9.9 × 9.9 μm pixel size and an 8-bit dynamic range. The focal length and the diameter of each microlens are 6.8 mm and 200 μm, respectively.

The peak intensity of a pulse is determined by its peak power and focal spot. The peak power is in turn determined by the energy and the temporal profile of a pulse which can be obtained from the spectrum and the autocorrelation function [8]. Experimentally registered spectra, autocorrelation functions of the amplified compressed pulses, and reconstructed temporal pulse profiles are shown in Fig. 2. Peak powers are 2.9 ± 0.1 TW and 4 ± 0.1 TW in the first and the second channels, respectively, with a pulse duration being 23 ± 1 and 24 ± 1 fs. The uncertainty in the peak power is determined by the slight shot-to-shot variations in the autocorrelation functions and the temporal profile reconstruction ambiguity [9].

Coherent combining requires that pulses are perfectly synchronized and phased. Thus, we have developed the synchronization setup (Fig. 1), the basic working principles of which are described elsewhere [5]. As discussed in detail in [5], if only amplified pulses with 10 Hz repetition rate are used in a stabilization setup, noise reduction in frequencies only lower than 1 Hz is possible. We suggest and implement a technique to improve stability of amplified pulses in low-repetition rate systems. The major idea is the usage for the stabilization not only amplified but also high-repetition rate unamplified part of radiation, that can allow considerable enhancement of the stabilization bandwidth and, consequently, synchronization improving. In [5], the increase of the stabilization bandwidth from 1 Hz to only about 10 Hz was realized. As have been found, the main problem was the low correlation between loops. Note that the usage of two loops for stabilization requires high correlation between them otherwise they act in different directions and stabilization becomes considerably worse. Previously, [5] amplified and unamplified pulses were sampled separately in different parts of the setup, which caused differences in their optical paths and, consequently, in registered phase errors and resulted in correlation decrease. We improved the stabilization setup (Fig. 1), and presently the amplified and unamplified pulses are sampled uniformly in the same place which resulted in correlation increase from 0.3 to 0.9 and more than ten times stabilization bandwidth enhancement. The measured time dependence of the phase difference and power spectral density of the phase noise are presented in Fig. 3. According to the data, the setup has 100 Hz stabilization bandwidth and allows achieving of a 85 mrad root mean square (RMS) relative phase instability

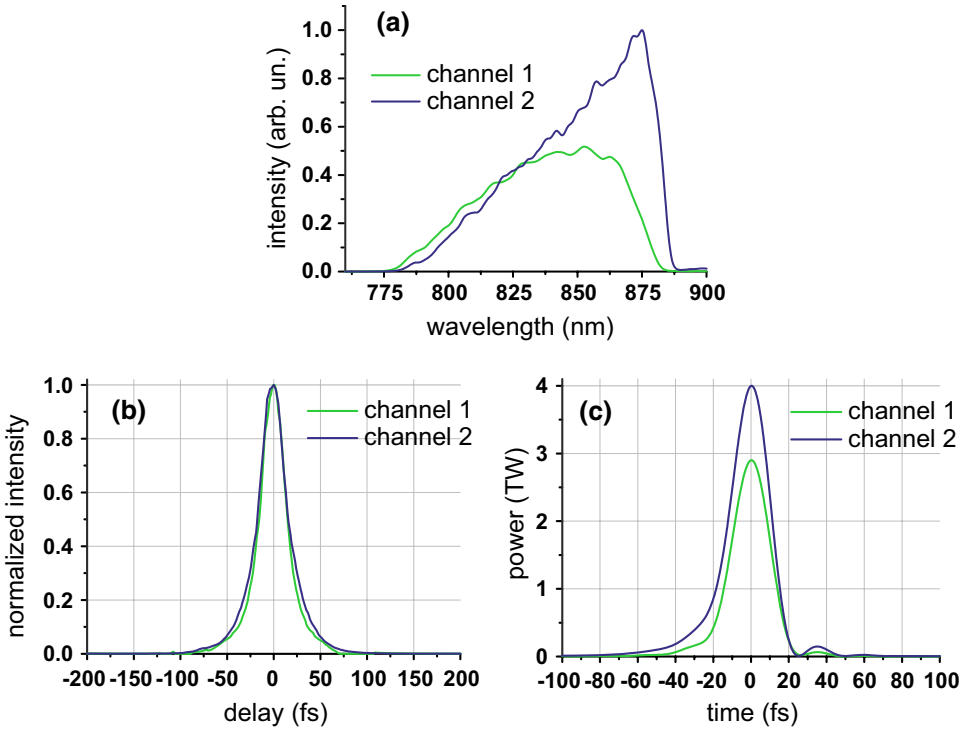

Fig. 2 Spectra (**a**), autocorrelation functions (**b**) and reconstructed power profiles (**c**) of amplified compressed pulses

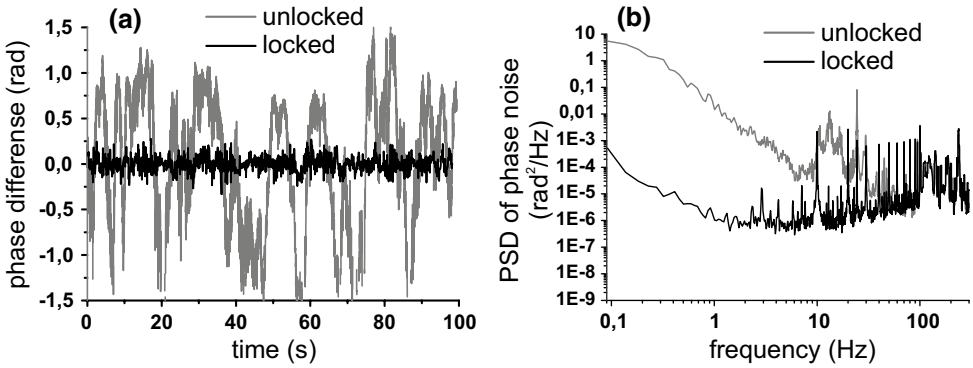

Fig. 3 Time dependence of phase difference (**a**) and power spectral density (PSD) of phase noise (**b**) registered in locked and unlocked regimes

of amplified pulses, which enables high-efficient coherent beam combining. It should be noted that the same approach can be used to considerably improve stability of not only phase difference but of almost all pulse parameters, for example of beam pointing [10].

Maximizing the focused intensity on a target is important for many applications, such as ultrafast X-ray sources, electron acceleration, and relativistic plasma physics. The wavefront distortions of a beam are critical in designing for an optimum intensity. So, we measure aberrations of the amplified beams. Note that a wavefront registered by the sensing configuration (Fig. 1b) contains the total sum of the beam aberrations and the parabolic mirror aberrations, which determine the focal intensity distribution and must be corrected to obtain the diffraction-limited focal spot [11]. The measured wavefronts are shown in Fig. 4. In the first channel, the RMS wavefront quality is 0.15λ, and peak-to-valley (PV) distance is 1.3λ. In the second channel, the corresponding values are 0.23λ and 2.7λ, respectively. The statistical RMS instability of the registered wavefronts is 0.01λ, which was calculated by averaging the RMS value of each wavefront relative to the mean wavefront shape using 20 shots. The expected focal spots of the individual beams and the combined beam (Fig. 5a–d) are calculated under the assumption of perfect pulse synchronization and using experimentally registered peak powers, wavefronts, and intensity distributions of the amplified pulses in front of the parabolic mirror. The Stratton–Chu vector diffraction theory [11, 12] is used to accurately calculate the electromagnetic field at the focus of the parabolic mirror with a high numerical aperture. The calculated peak intensities are 2.4×10^{19}, 3.93×10^{19}, and 1.18×10^{20} W/cm^2 for the

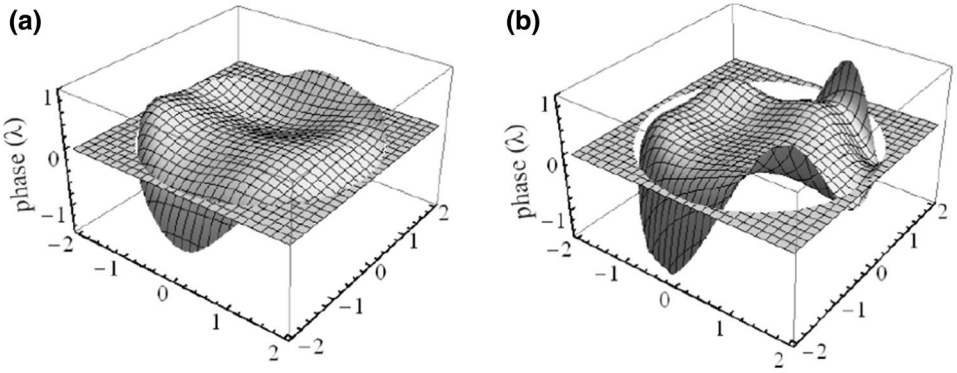

Fig. 4 Experimentally registered wavefronts in the first (**a**) and the second (**b**) channels

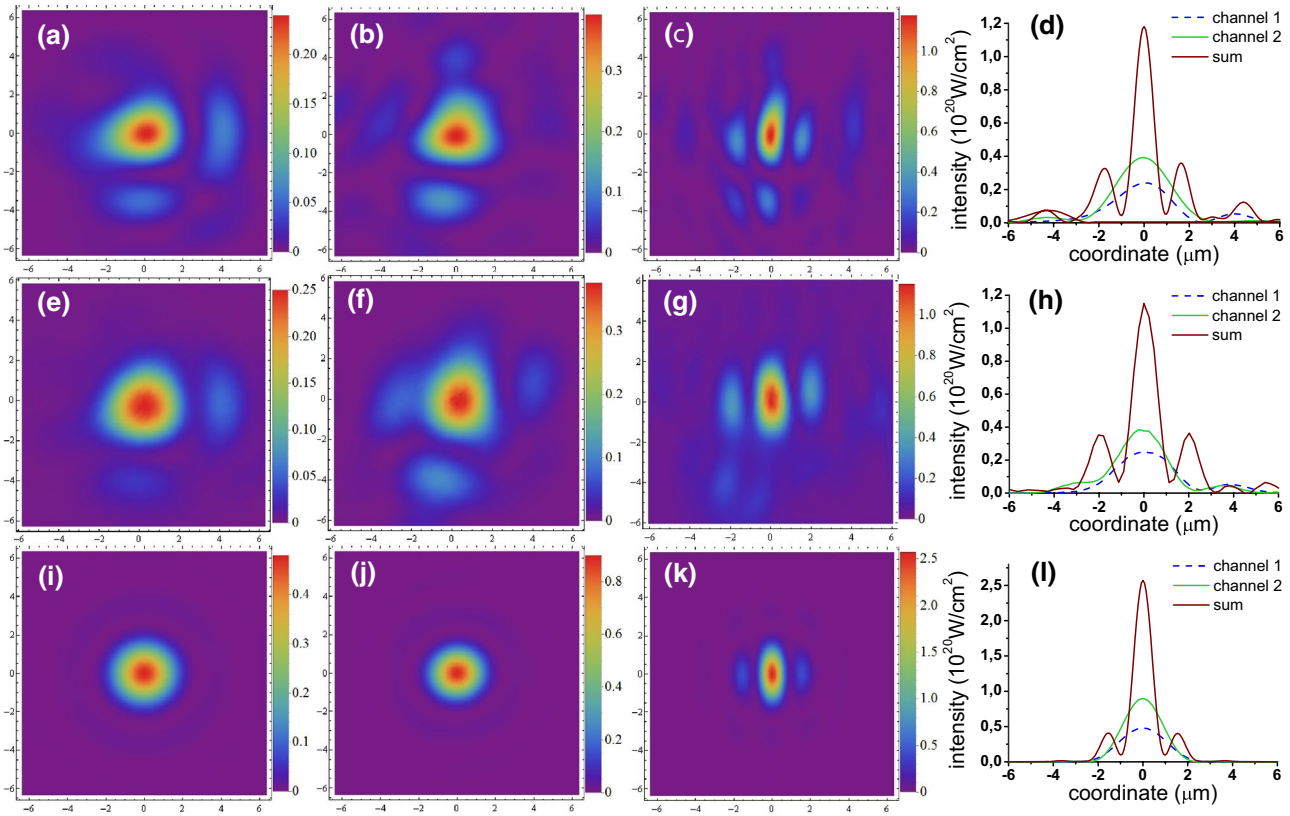

Fig. 5 Calculated using measured near-field intensity and phase distributions (**a**–**d**), experimentally registered (**e**–**h**) and diffraction-limited (**i**–**l**) focal spots for the first channel (**a**, **e**, **i**), the second channel (**b**, **f**, **j**), the combined beam (**c**, **g**, **k**), and horizontal data projection (**d**, **h**, **l**). (all coordinates are given in μm; FWHM beam sizes: **a** 2.8 × 2.3 μm; **b** 2.6 × 2.7 μm; **c** 1 × 2.5 μm; **e** 2.7 × 2.6 μm; **f** 2.4 × 2.7 μm; **g** 1.1 × 2.5 μm; **i** 2.3 × 2.3 μm; **j** 2 × 2 μm; **k** 0.9 × 2.1 μm)

first channel, the second channel, and the combined beam, respectively.

The experimentally registered focal intensity distributions for both channels are shown in Fig. 5e, f. The image resolution is 12 pixels per beam diameter (2.7 μm). As follows from the registered peak powers and focal spots, relativistic intensities of $I_1 = 2.5 \times 10^{19}$ W/cm^2 and $I_2 = 3.76 \times 10^{19}$ W/cm^2 are achieved in the first and the second channels, respectively. Coherent combining is primarily implemented because preserving the focusing mirror and beam parameters, it allows the enhancement of peak intensity by nearly the squared number of channels; however, this enhancement is only possible until the mirror aperture is completely filled. In our case, peak intensity can be increased up to $I_{\Sigma\max} = 1.24 \times 10^{20}$ W/cm^2, where

$$I_{\sum}\max = \left(\sum_{n=1}^{2}\sqrt{I_n}\right)^2 \quad (1)$$

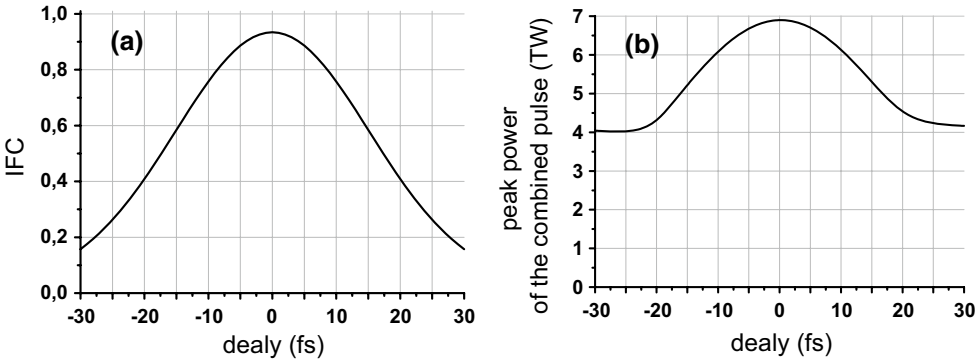

Fig. 6 Dependence of the interference figure contrast (IFC) (**a**) and of the peak power of the combined pulse (**b**) on the delay between pulses from the first and the second channels

The experimentally registered focal intensity distribution of the combined beam is shown in Fig. 5g. The FWHM size of the beam in the interference direction decreases to 1.1 versus 2.7 μm for a single beam. In the implemented tiled aperture combining, a peak power of the combined pulse is determined by peak powers and time distributions of the individual pulses and the delay between them. The delay is set by the synchronization setup to nearly zero. And the accuracy of the beam overlap in the time domain can be evaluated from the interference figure contrast (IFC). The IFC is defined by the formula

$$\mathrm{IFC} = \frac{I_{\max} - I_{\min}}{I_{\max} + I_{\min}} \tag{2}$$

where $I_{\max}$ and $I_{\min}$ are the maximum and the adjacent minimum on the intensity pattern, respectively. The numerically calculated dependence of IFC on the delay between the pulses is shown in Fig. 6a. This calculation takes into account experimentally registered spectra, energies, and profiles of the pulses. Note that the IFC is less than unity for a zero delay because of differences in energies, peak powers, and spectra of the combined pulses. The IFC in Fig. 5g is 0.9, which corresponds to a delay that does not exceed 4 fs. The computed dependence of the combined pulse peak power on the delay between individual pulses is presented in Fig. 6b. As follows from the data, the delay error of 4 fs corresponds to a peak power of the combined pulse of at least 6.8 TW, with the pulse duration being 23.5 fs. Obtained parameters of the combined pulse almost coincide with ultimate values achievable under the perfect synchronization which are 6.9 TW and 23.2 fs, respectively. And the peak intensity of the combined pulses is $I_{\Sigma} = 1.15 \times 10^{20}$ W/cm^2. The performance of the coherent combining can be characterized by an efficiency (η) defined as follows: [5, 13]

$$\eta = \frac{I_{\sum}}{I_{\sum \max}} \tag{3}$$

The efficiency of the coherent combining of 93 % is achieved in the experiments.

The measured and calculated peak intensities are within 4.5 % of each other and are thus in good agreement. There is also a good agreement between the measured and the calculated intensity distributions at the focus. In particular, the registered and the calculated FWHM focused beam sizes are within 4–8 % of each other. These results show that the developed pulse characterization technique is sufficiently accurate.

It should be noted that further peak intensity increase can be realized by enhancing the numerical aperture of a focusing element, for example, by replacing the *f*/1.2 parabolic mirror with *f*/0.6 one [11]. According to our calculations, a *f*/0.6 parabolic mirror enables the increase of the peak intensity of the combined beam to 3.5×10^{20} W/cm^2 using the same beams, and aberrations' compensation provides additional twice increase.

The focused intensity is frequently qualified in terms of the normalized Strehl ratio, which is the ratio of the intensity at the focus of a beam with a distorted wavefront to a beam with a flat wavefront and the same near-field intensity distribution. A nearly flat phase front can be obtained by providing feedback to deformable mirrors using measured wavefronts [11]. Calculated diffraction-limited focal intensity distributions are presented in Fig. 5i–l. In this case, peak intensities are 0.48×10^{20}, 0.9×10^{20}, and 2.57×10^{20} W/cm^2 for the first channel, the second channel, and the combined beam, respectively. Thus, Strehl ratios of 0.52 and 0.42 are achieved for the first and the second channels, respectively. Note that it is realized without any wavefront correction setup.

Obtained result can become one of the milestones on the road toward ultra-relativistic intensity. For instance, assuming 1 PW peak power which is already nearly achieved in the systems based on parametric amplification in LBO [14] and DKDP [15] crystals combining of 10 beams will provide ultra-relativistic intensity of $10^{24–25}$ W/cm^2. Note that achievement of as high peak intensity as possible requires

proper adjustment of beam mode and polarization features [16, 17].

In conclusion, we have experimentally demonstrated coherent combining of relativistic-intensity femtosecond pulses for the first time. The original stabilization setup developed by us provides 100 Hz stabilization bandwidth and a 85 mrad root mean square relative phase instability of amplified pulses. The peak intensity of the combined beam of 1.15×10^{20} W/cm^2 and the combining efficiency of 93 % are achieved using a *f*/1.2 parabolic mirror. A Strehl ratio of 0.42–0.52 is obtained without any wavefront correction setup. Peak intensity can be further increased up to 0.7×10^{21} W/cm^2 by aberrations correction implementation and using a *f*/0.6 parabolic mirror.

This work has been partly supported by the Russian Academy of Sciences under the Program of Basic Research "Extreme Light Fields and Their Applications".

References

1. G.A. Mourou, T. Tajima, S.V. Bulanov, Rev. Mod. Phys. **78**, 309 (2006)
2. ELI—Extreme Light Infrastructure, *White Book*. http://www.eli-beams.eu/wp-content/uploads/2011/08/ELI-Book_neues_Logo-edited-web.pdf
3. Exawatt Center for Extreme Light Studies (XCELS), *Project Summary*. http://www.xcels.iapras.ru/img/site-XCELS.pdf
4. Ultra-high Intensity Laser Initiative at the University of Rochester's Laboratory for Laser Energetics. https://www.burning-plasma.org/web/fesac-fsff2013/whitepapers/Meyerhofer_D.pdf
5. S.N. Bagayev, V.E. Leshchenko, V.I. Trunov, E.V. Pestryakov, S.A. Frolov, Opt. Lett. **39**, 1517 (2014)
6. V.E. Leshchenko, V.I. Trunov, S.A. Frolov, E.V. Pestryakov, V.A. Vasiliev, N.L. Kvashnin, S.N. Bagayev, Laser Phys. Lett. **11**, 095301 (2014)
7. V.E. Leshchenko, V.I. Trunov, E.V. Pestryakov, S.A. Frolov, Atmos. Ocean. Opt. **27**, 571 (2014)
8. J.-C. Diels, W. Rudolph, *Ultrashort Laser Pulse Phenomena: Fundamentals, Techniques, and Applications on a Femtosecond Time Scale* (Academic Press, San Diego, 2006)
9. J.-H. Chung, A.M. Weiner, IEEE J. Sel. Top. Quantum Electron. **7**, 656 (2002)
10. G. Genoud, F. Wojda, M. Burza, A. Persson, C.-G. Wahlström, Rev. Sci. Instrum. **82**, 033102 (2011)
11. S.-W. Bahk, P. Rousseau, T.A. Planchon, V. Chvykov, G. Kalintchenko, A. Maksimchuk, G.A. Mourou, V. Yanovsky, Appl. Phys. B **80**, 823 (2005)
12. P. Varga, P. Török, J. Opt. Soc. Am. A: **17**, 2081 (2000)
13. C.X. Yu, S.J. Augst, S.M. Redmond, K.C. Goldizen, D.V. Murphy, A. Sanchez, T.Y. Fan, Opt. Lett. **36**, 2686 (2011)
14. L. Xu, L. Yu, X. Liang, Y. Chu, Z. Hu, L. Ma, Y. Xu, C. Wang, X. Lu, H. Lu, Y. Yue, Y. Zhao, F. Fan, H. Tu, Y. Leng, R. Li, Z. Xu, Opt. Lett. **38**, 4837 (2013)
15. V.V. Lozhkarev, G.I. Freidman, V.N. Ginzburg, E.V. Katin, E.A. Khazanov, A.V. Kirsanov, G.A. Luchinin, A.N. Malshakov, M.A. Martyanov, O.V. Palashov, A.K. Poteomkin, A.M. Sergeev, A.A. Shaykin, I.V. Yakovlev, Laser Phys. Lett. **4**, 421 (2007)
16. C.J.R. Sheppard, N.K. Balla, S. Rehman, Opt. Commun. **282**, 727 (2009)
17. A.V. Bashinov, A.A. Gonoskov, A.V. Kim, G. Mourou, A.M. Sergeev, Eur. Phys. J. Spec. Top. **223**, 1105 (2014)